Pergamon

Journal of Structural Geology, Vol. 16, No. 10, pp. 1477 to 1490, 1994

0191-8141/94 $7.00+0.00

0191-8141(94)E0003-H

A simple kinematic model for crustal deformation along two- and three-dimensional listric normal faults derived from scaled laboratory experiments

JEAN BRAUN, GEOFFREY E. BATT, DEBORAH L. SCOTT, HERBERT MCQUEEN and ANTHONY R. BEASLEY

Research School of Earth Sciences, Australian National University, Canberra, A.C.T., 0200, Australia

(*Received* 7 *May* 1993; *accepted in revised form* 1 *December* 1993)

Abstract—We have derived a simple kinematic model of the deformation that results from extension accommodated by movement of a crustal block along two- and three-dimensional listric fault surfaces. The model accurately reproduces deformation observed in a series of scaled analogue models. The kinematic model is based on the simple assumption that lines within the hangingwall that are normal to the fault surface before deformation remain so following deformation. An additional constraint built into the model is that of incompressibility.

Deformation in the hangingwall block as observed in the laboratory experiments and predicted by the kinematic model is characterized by: (1) a key-stone structure (or crestal-collapse graben) at some finite distance from the fault tip; and (2) pure solid-body rotation of the hangingwall head area near the tip of the fault. In three dimensions, the central region of the model undergoes extension in a direction normal to the direction of imposed displacement in such a way that the direction of dip of the upper surface of the hangingwall is aligned with the direction of extension. This result provides quantitative support for the use of dip analysis to infer tectonic transport direction. We also show how the distribution of extension within the hangingwall is affected when the constraint of constant displacement along the fault is relaxed.

INTRODUCTION

CRUSTAL extension is accommodated by movement along discrete, often listric, normal faults. In many instances, the exact fault geometry is poorly constrained and, therefore, the nature and amount of extension must be derived from the geometry of originally-flat marker horizons within the hangingwall (Verral 1981) or within the overlying sedimentary section. To be accurate, this approach must be based on a proper understanding of the internal deformation of the hangingwall and how it relates to the fault geometry. Several geometrical models have been proposed that relate the geometry of the hangingwall surface to the geometry of the fault surface and the amount of extension (e.g. Dula 1991). The vertical shear model (Verral 1981), the inclined shear model (White *et al.* 1986) and the slip-line model (Williams & Vann 1987) are just a few examples. Most of these models are characterized by their relative simplicity which makes them particularly suitable for direct use on migrated seismic sections.

Although some models have been successful at accurately predicting fault geometries in natural or synthetic test cases (Dula 1991), it is quite puzzling that apparently none of them is capable of reproducing the deformation patterns observed in scaled laboratory experiments (McClay & Ellis 1987a,b) or in the field. Indeed, in cases where friction along the fault is neglected, sandbox models predict that hangingwall deformation is accommodated by extension localized at the crest of the rollover anticline (Fig. 1a) whereas the head of the hangingwall rotates but remains undeformed. This concentration of deformation in the hangingwall appears to be independent of the material used in the experiments (McClay 1989), suggesting a purely geometrical rather than mechanical control. Similar features encountered in the field have led to the suggestion that localized extension in the hangingwall block reflects the geometry of the listric fault and must therefore indicate a local

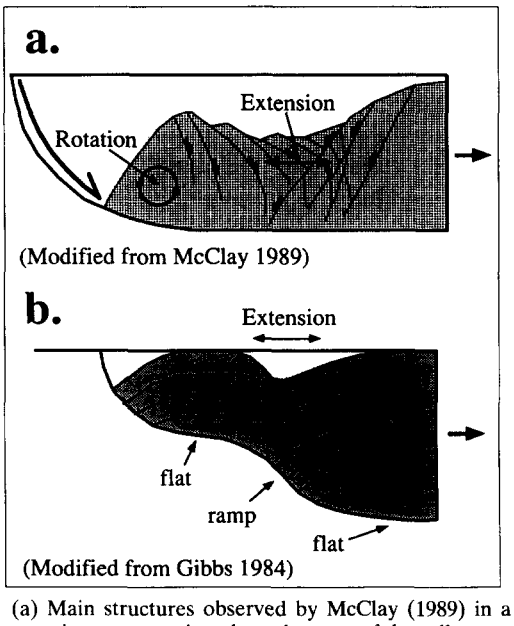

Fig. 1. (a) Main structures observed by McClay (1989) in a deformation experiment: extension along the crest of the rollover anticline and rotation of the hangingwall toe. (b) Conceptual model of the deformation of a crustal block sliding along a listric normal fault made of a succession of ramps and flats.

change in the fault surface geometry (Gibbs 1984) (Fig. 1b).

In this paper, we present the results of a series of scaled laboratory experiments designed to address the problem of hangingwall deformation during crustal extension along two- and three-dimensional listric fault surfaces. The results of the experiments are then interpreted and used as the basis for a new kinematic model based on what we term the 'rule of the normal'. We also show how the constraint of incompressibility can be easily incorporated into the model. We investigate the effect of relaxing the condition of constant displacement along the fault surface on the distribution of deformation in the hangingwall. Finally, we use the kinematic model to provide a quantitative support for the use of dip analysis for inferring regional kinematic histories in areas of non-ideal extension (Scott *et al.* 1994).

EXPERIMENTAL METHOD

Apparatus

The experimental program was carried out in two Perspex deformation rigs designed to simulate different detachment surface orientations relative to the direction of extension. The first series of experiments was carried out in an effectively two-dimensional deformation rig measuring 50 × 30 × 10 cm (Fig. 2a). The detachment surface is a simple ramp structure shaped as an exponential curve with a decay constant of 5 cm. In plan, the trace of the surface is aligned perpendicular to the direction of extension so that only normal movement, with no strike-slip component, could occur on it, similar to previous sandbox experiments (e.g. McClay & Ellis 1987a,b, Ellis & McClay 1988, McClay 1989). The modelling rig for the second series of experiments differed from this in that the detachment surface was composed of two symmetrical halves, which we will later refer to as 'segments', oriented at 45° to the direction of extension (Fig. 2b).

The detachment surfaces in these models were moulded from Perspex to the desired shape and attached to the fixed walls of the deformation rig. Extension was achieved using a thin sheet of mylar overlying the surfaces and attached to a motor driven roller which gave a constant displacement rate of 10 cm h^{-1} (approximately 2.77 × 10^{-3} cm s^{-1}). The rigid nature of the detachment surfaces effectively limited deformation to the hangingwall above them. In the two-dimensional experiment, the mylar sheet could be simply cut to fit the detachment surface. However, in the more complicated three-dimensional case, the changing area and shape of the detachment surface going from the curved 'head region' in the corner formed by the fault segments, to the flat area of the deformation rig, required a series of slits and overlapping segments to be added to the mylar sheet to allow it to fan out or contract as required without buckling or otherwise disturbing the overlying block of material.

The analogue hangingwall consisted of multiple layers of homogeneous 250–500 μm diameter sand with an angle of internal friction of 33.5° constructed by adding sand to the rig and carefully levelling it at the desired thicknesses. Marker horizons and a grid of coloured sand on the surface of the models enabled internal and surface deformation to be evaluated. The sand used was effectively cohesionless and isotropic. However, the extensive analogue modelling work of Ellis & McClay (1988) suggests that, in the case of a listric detachment surface, the structures formed are effectively independent of the materials used, and thus, the results of the experiments presented here are probably generally applicable.

Experiments were continued only until freely cascading surfaces began to develop in the sand (i.e. as slopes reached 33.5°). Deformation was recorded primarily using 35 mm time-lapse still photography through the clear sides of the deformation rig. Oblique and plan views were also recorded to study the development of surface features.

The effect of friction along the vertical sides of the

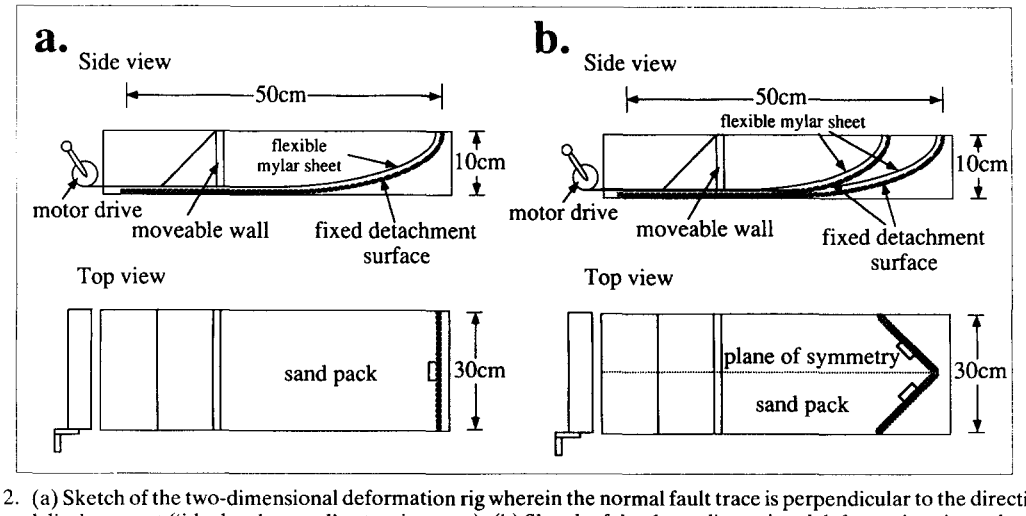

Fig. 2. (a) Sketch of the two-dimensional deformation rig wherein the normal fault trace is perpendicular to the direction of imposed displacement ('ideal orthogonal' extension case). (b) Sketch of the three-dimensional deformation rig made of two symmetrical fault surfaces oriented at 45° with respect to the direction of displacement ('non-ideal' extension case).

deformation rig was investigated in one of the experiments. An additional piece of mylar was added between the sand pack and one of the sidewalls and was forced to move with the sand pack. An additional piece of mylar coated with sand was attached to the deformation rig on the other side of the sand pack. Thus, friction was reduced along one side of the sand pack and enhanced on the other side. The deformation patterns observed through both sidewalls were slightly translated in the direction of imposed displacements but otherwise almost identical to those formed in a similar experiment where the sand pack was forced to slide directly against the sidewalls of the deformation rig.

Scaling

In selecting an appropriate material to simulate tectonic processes in analogue modelling experiments, the effect of scaling on physical parameters must be appreciated (Hubbert 1937, Horsfield 1977). In the experiments described here, a 10 cm deep model is used to represent deformation in the upper 1–10 km of the Earth's crust, giving a reduction in scale by a factor of 10^{-4}–10^{-5}. Thus, for typical crustal rocks with a cohesive strength of 5–10 MPa, the corresponding modelling material should have a cohesive strength of the order of 10–20 Pa (Hubbert 1937). This value is so small in comparison to the principal stress values in the model that a cohesionless material such as loose sand can reasonably be used as the modelling medium (Horsfield 1977). However, it should be noted that the size of sand grains used in the analogue experiment is not scaled properly (Ellis & McClay 1988), resulting in the production of shear zones in the analogue model, rather than discrete fault planes.

The angle of internal friction is a dimensionless quantity, and is thus not affected by the scaling of the model. The angle of internal friction of the sand used in the experiments (33.5°) falls within the range of experimentally obtained values for typical crustal gneisses, which range from 35.4° for dry to 31.4° for wet conditions (Jaeger & Cook 1979).

TWO-DIMENSIONAL MODEL RESULTS

The deformation pattern observed in repeated experimental runs of the two-dimensional model can, like that recorded in similar experiments by Ellis & McClay (1988), be broken up into three regions of varying behaviour (Fig. 3a):

—the proximal region (P) of the hangingwall, originally overlying the steep section of the fault (S), is characterized by pure solid-body rotation;

—the distal region (D) of the hangingwall, originally overlying the flat section of the fault (F), has undergone pure solid-body translation;

—the transitional region (T) of the hangingwall, between regions P and D and originally overlying the intermediary section of the fault (I), has undergone horizontal extension and bending.

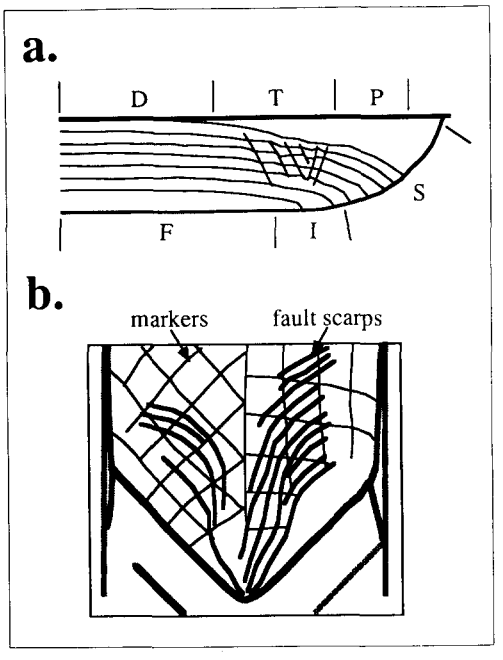

Fig. 3. Sketch of the results of one of the two- and three-dimensional experiments. (a) Line drawing of major structures observed through the side wall in one of the two-dimensional experiments. We distinguish proximal (P), transitional (T) and distal (D) regions of the hangingwall and steep (S), intermediary (I) and flat (F) sections of the fault surface. (b) Interpretation of the results of one of the three-dimensional experiments seen from above. The dark thick lines are interpreted normal faults; the dashed thin lines are the post-deformation position of an initially regular grid marked on the sand surface. On the left-hand side of the bisector, the grid was drawn parallel to the fault surface trace whereas on the right-hand side, the grid was drawn parallel to the edges of the experimental 'box', or the direction of displacement.

Region P has a horizontal dimension of approximately 80 mm, or about 80% of the thickness of the hangingwall. It undergoes very little internal deformation, as shown in Figs. 4(a) & (b). In region T, the model passes into a roll-over antiform, which coincides with the development of a complex crestal collapse graben. The graben is approximately 120 mm wide, or 120% of the hangingwall thickness, and is bounded by at least three pairs of conjugate planar normal faults dipping at angles of 55–60°. These faults break the surface of the hangingwall and produce a series of prominent 'fault scarps' on the surface of the model (Fig. 4b). In region D, the model is deformed by simple, non-rotating, solid-body translation with very little apparent internal deformation.

THREE-DIMENSIONAL MODEL RESULTS

The deformation pattern produced in the three-dimensional modelling experiments is bilaterally symmetrical about the centre line of the deformation rig (Figs. 3b and 4c). The surface of each of the mirror-image halves is marked by a similar tripartite division of features as seen in the two-dimensional modelling experiments discussed above. In detail, the surface deformation is characterized by:

—two very flat-surfaced proximal regions, P1 and P2, apparently deforming by solid-body rotation;

—two distal regions, D1 and D2, deforming by solid–body translation;

—two transitional regions, T1 and T2, characterized by normal fault scarps the strikes of which suggest that extension in regions T1 and T2 is aligned with the direction of maximum dip of each fault segment;

—a central region, C, comprising the 'beak' of the hangingwall, characterized by surface fault scarps aligned with the direction of imposed displacement, therefore indicating that extension in region C is perpendicular to the direction of imposed displacement.

Overall, the observed structural pattern in the three-dimensional model is suggestive of twin sets of the features seen in the two-dimensional experiments. Each set is associated with one of the fault surfaces but they appear to interfere with one another in the middle of the deformation rig. In region C, the surface is far more steeply dipping parallel to the side walls, and hence to the direction of extension, than perpendicular to the side walls of the deformation rig (measured slopes in this latter direction range from 3° to 5°).

INTERPRETATION OF EXPERIMENTAL RESULTS

The results of the two-dimensional experiments show that maximum deformation within the sand pack does not take place in regions located initially above sections of the fault where curvature is maximum (region P). Rather, deformation is most intense near the surface at a finite distance from the fault tip (region T). Almost identical deformation patterns were produced by Ellis & McClay (1988) and McClay (1989). Their use of a wide array of modelling materials demonstrates that hangingwall deformation is strongly controlled by the geometry of the listric detachment. However, no general kinematic model like the so-called 'chevron' construction of Verrall (1981), has yet been presented to demonstrate how movement along a listric fault of constantly decreasing curvature can produce localized extension at the surface of the deforming hangingwall at some finite distance from the tip of the fault. In the following section, we develop a kinematic model which accurately predicts the deformation observed in the experimental models.

A simple kinematic model: the rule of the normal

The analogue experiments we performed, although meant to represent movement of a crustal block along a normal listric fault, are in fact equivalent to deforming the hangingwall by unfolding its curved base as shown in Fig. 5. Indeed, the mylar sheet inserted between the sand and the rigid fault is unstretchable, so the base of the hangingwall experiences no strain in a direction tangent to the fault surface as a result of drag on the detachment surface. From this simple observation, one may deduce a rather general deformation law within the hangingwall: because the internal deformation of the hangingwall is driven solely by bending imposed along its base, it is natural to assume, as in plate bending theory, that a line normal to the base of the hangingwall remains normal to the base of the hangingwall, even after finite deformation. This purely geometrical rule, which we named the 'rule of the normal', is equivalent to Kirchoff's hypothesis that serves as the basis of the theory of thin plate bending (Fung 1963, p. 458). It is also identical to the slip-line construction of Williams & Vann (1987) in the limit of infinitesimal displacements.

It is important to note that the rule of the normal can only be used in situations where one, and only one, normal to the fault surface passes through any given point within the hangingwall. If, for instance and as pointed out by Wheeler (1987), the fault curvature is such that a region of the hangingwall is at a distance from the fault surface greater than the local radius of curvature of the fault, the rule of the normal becomes ambiguous.

We can use the rule of the normal to describe the path followed by a particle within the hangingwall from its original position $x_0(X)$ to its final position $x_1(X)$. x_0 and x_1 are spatial co-ordinates measured in a system of co-ordinates that is fixed in space; X are material co-ordinates attached to the deforming body. Although the rule of the normal is conceptually very simple, its practical implementation, as demonstrated below, is not always straightforward.

As an example, consider particle A in Fig. 6(a) that is located at $x_0(A)$ before deformation, a distance r from the fault surface. To find its final location after the hangingwall has been moved by a distance u_0, first project A normally to the fault surface to point A', then translate it along the fault surface by an amount u_0, measured as a distance along the fault, to position A'' and finally project it back to A''' in such a way that it is still located at a distance r from the fault surface. Note that the distance along a curved surface parameterized by $z = f(x)$ is given by:

$$u_0 = \int_x^{x+\Delta x} \sqrt{1 + \left(\frac{\partial f(x)}{\partial x}\right)^2}\, \mathrm{d}x. \qquad (1)$$

Therefore, to find the increment in horizontal co-ordinate, Δx, that corresponds to a given displacement u_0 along the surface, one must solve a first-order integral equation in x.

Particle B, originally an infinitesimal distance $\mathrm{d}l$ from A but at the same distance r from the fault, will follow a similar but not identical path as shown in Fig. 6(a). The distance between A' and B' is:

$$\mathrm{d}l' = \frac{\mathrm{d}l}{\left(1 - \frac{r}{\Gamma_1}\right)}, \qquad (2)$$

where Γ_1 is the radius of curvature of the fault in the vicinity of A' and B'. The translation along the fault is

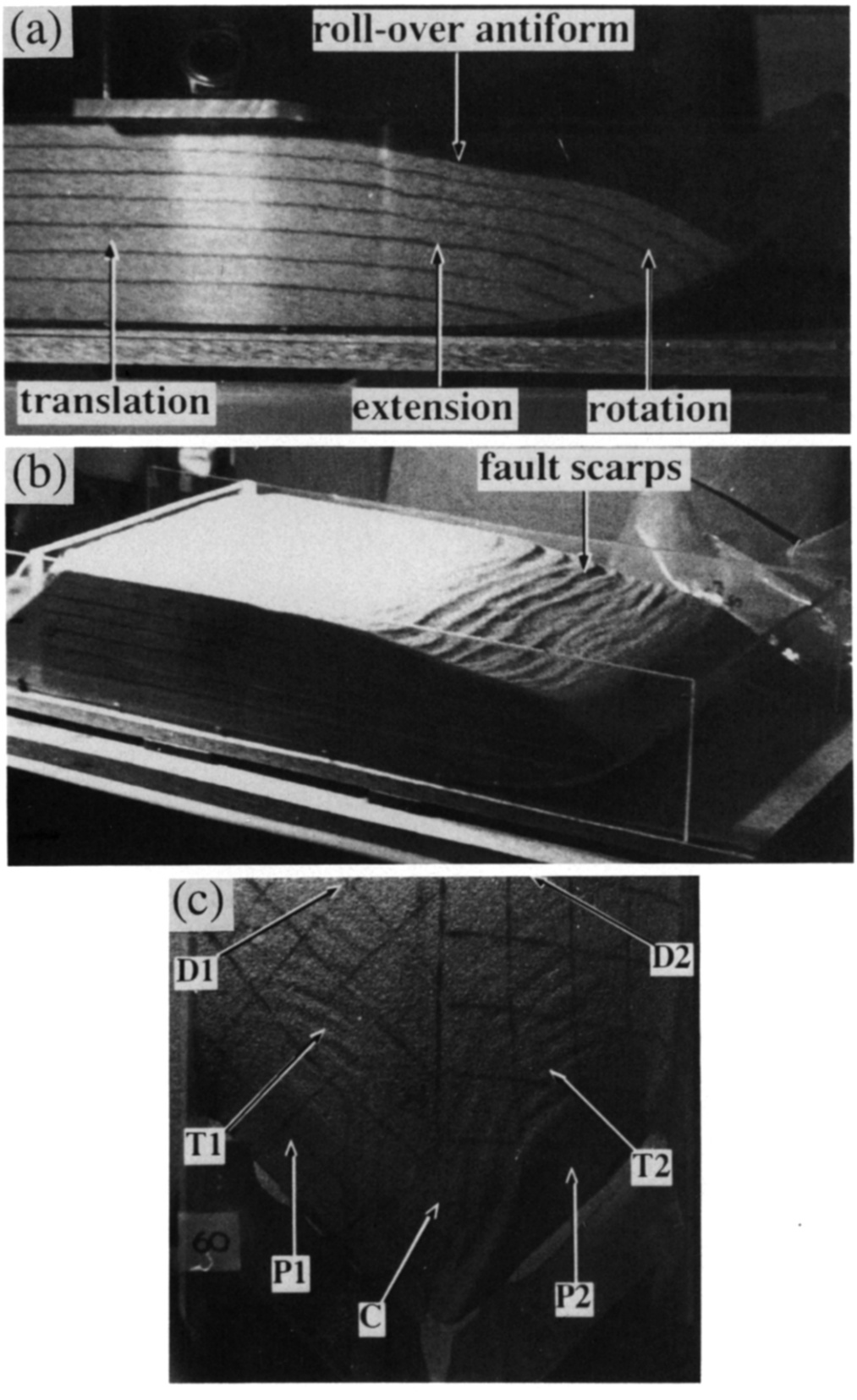

Fig. 4. Results of one of the two- and three-dimensional experiments. (a) Two-dimensional experiment. Side view of the deformed sand pack seen through the transparent side of the deformation rig. (b) Two-dimensional experiment. Oblique view of the sand pack under oblique lighting to highlight the surface fault scarps. (c) Three-dimensional experiment viewed from the top; the illumination is from the upper left corner. The results are almost symmetrical with respect to the bisector plane of the two fault surfaces; the apparent asymmetry is due to the oblique illumination. The distal (D1 and D2), transitional (T1 and T2), proximal (P1 and P2) and central (C) regions of the hangingwall are labelled.

the same for points A' and B' and therefore $dl'' = dl'$. The distance between A''' and B''' is:

$$dl''' = dl''\left(1 - \frac{r}{\Gamma_2}\right), \tag{3}$$

where Γ_2 is the radius of curvature of the fault in the vicinity of A'' and B''. The total stretch in a direction tangent to the fault surface, Λ_0, is therefore given by:

$$\Lambda_0 = \frac{dl}{dl'''} = \frac{1 - \frac{r}{\Gamma_2}}{1 - \frac{r}{\Gamma_1}}. \tag{4}$$

The radius of curvature, Γ, of a curve described by $z = f(x)$ is:

$$\Gamma = \frac{\left[1 + \left(\frac{\partial f}{\partial x}\right)^2\right]^{3/2}}{\frac{\partial^2 f}{\partial x^2}}. \tag{5}$$

The line joining A and B also undergoes finite rotation during the deformation of the sand pack. Following the rule of the normal, the rotation, Ω_0, is given by the dot product of the unit normals to the fault (Fig. 6a) at locations $A'(n_1)$ and $A''(n_2)$:

$$\Omega_0 = \arccos(n_1 \cdot n_2). \tag{6}$$

Note that the direction of the normal to a curve represented by $z = f(x)$ is given by $n = [-(\partial f/\partial x), 1]$.

The stretch, Λ_0, and rotation, Ω_0, are in fact the principal components of second-order tensors, Λ and Ω, that are defined as the symmetrical and anti-symmetrical parts, respectively, of the deformation gradient tensor, $F = (\partial X/\partial z)$. The deformation gradient conceptually measures the difference in path followed by two material points initially next to each other.

Following the method described above, we have estimated the stretch, Λ_0, and rotation, Ω_0, for a series of points originally located at the nodes of a rectangular grid across the hangingwall. The listric fault is represented by an exponential curve of the form:

$$z = f(x) = -z_0\left[1 - \exp\left(-\frac{x}{\lambda}\right)\right], \tag{7}$$

where x and z are the horizontal and vertical coordinates, respectively, z_0 is the depth to detachment, and λ is the 'listricity' of the fault. The results, shown in Fig. 7, can be summarized as follows: (1) the proximal region of the hangingwall does not deform internally but undergoes a large amount of rotation; (2) the region of maximum extension is located at the surface of the sand pack at the top of an antiform developing in the transitional region of the hangingwall; and (3) extension rapidly decreases to become negligible in the distal region of the hangingwall. Comparing the kinematic model results with the analogue model results shown in Fig. 3, we find that the simple kinematic model has reproduced all of the large-scale characteristics of the deformation field observed in the laboratory experiment.

Location of the crestal graben

The kinematic model, based on the rule of the normal, demonstrates that movement on a simple listric fault gives rise to strain localization away from the fault tip. This point may be explicitly demonstrated as follows: we assume that the hangingwall has been displaced by a distance $u > \lambda$, such that the hangingwall is now located over the flat section of the fault where the local radius of curvature is very large ($\Gamma \to \infty$ as $(\partial 2f/\partial x2) \to 0$). A point on the surface of the hangingwall, originally at location [xs, 0] and a distance rs from the fault (Fig. 6b), experiences a finite stretch, Λs, given by:

$$\Lambda_s = \frac{1}{1 - \frac{r_s}{\Gamma_f}}, \tag{8}$$

where Γ_f is the local radius of curvature of the fault at the point $[x_f, f(x_f)]$, the normal projection of $[x_s, 0]$ onto the fault. The quantities x_s, Γ_f and r_s may all be expressed in terms of x_f, $f(x_f)$ and its derivatives in the following manner:

$$x_s = x_f + f\frac{\partial f}{\partial x}$$

$$r_s = -f\sqrt{1 + \left(\frac{\partial f}{\partial x}\right)^2} \tag{9}$$

$$\Gamma_f = \frac{\left[1 + \left(\frac{\partial f}{\partial x}\right)^2\right]^{3/2}}{\frac{\partial^2 f}{\partial x^2}}.$$

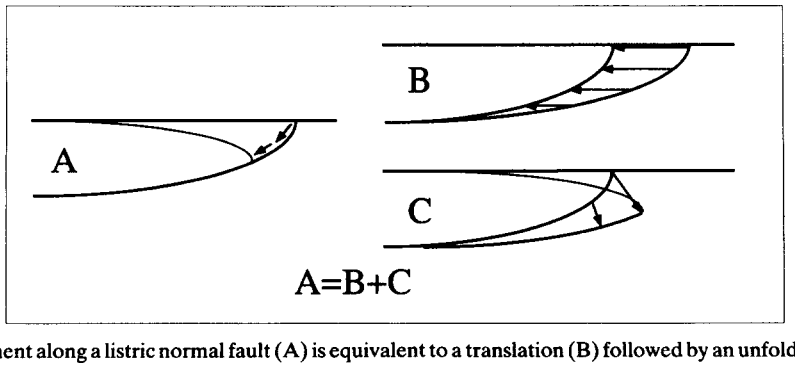

Fig. 5. Movement along a listric normal fault (A) is equivalent to a translation (B) followed by an unfolding of the base (C).

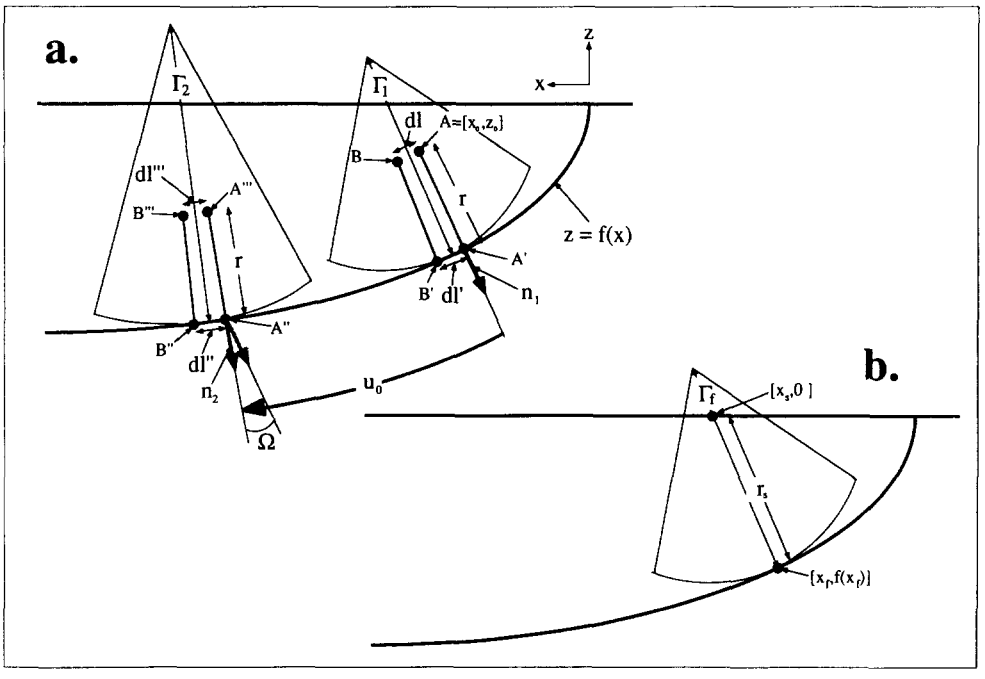

Fig. 6. (a) Geometrical construction used in the rule of the normal. Two material points (A and B) originally at the same distance r from the fault surface and a distance dl from each other follow slightly different paths as a result of internal deformation of the hangingwall. The local stretch resulting from the displacement of the hangingwall is given by the ratio of dl and the new distance between the same material points (now at A''' and B'''), dl'''. The rotation, Ω, is given by the dot product of the local normal to the fault, n_1, before deformation and, n_2, after deformation. A radius of curvature (Γ_i) may be defined at each point along the fault surface. (b) Geometrical parameters used to calculate the location of the roll-over antiform or crestal graben following finite displacement of the hangingwall.

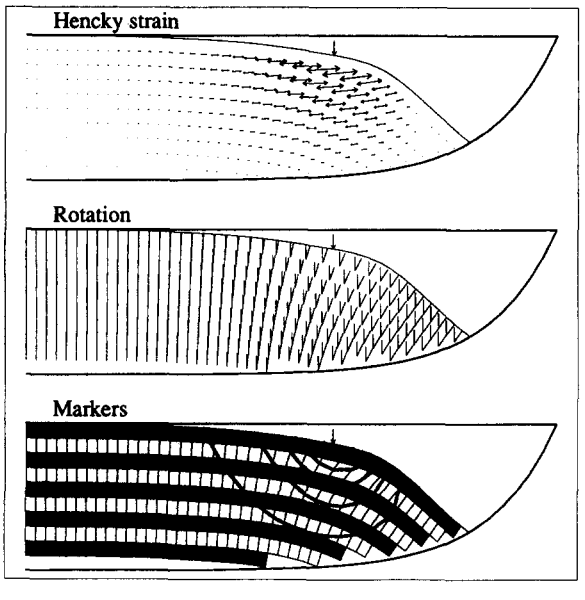

Fig. 7. Results of the kinematic model (to be compared with the results of the two-dimensional sand box experiment of Figs. 3a and 4a). (a) Distribution of deformation in the deformed sand pack; the arrows are aligned along the direction of the local maximum stretch component and their amplitude is given by the value of the Hencky strain, $\varepsilon = \ln \Lambda_0$. (b) Distribution of material rotation in the deformed sand pack. At any given point, the rotation angle is given by the angle between a vertical line and the position of a material line that was vertical in the undeformed configuration. (c) Geometry of an initially rectangular grid following deformation; the dark lines are contours of constant stretch. The small vertical arrow indicates the location of the maximum surface extension as computed from the rule of the normal.

The total stretch Λ_s is therefore given by:

$$\Lambda_s = \frac{1 + \left(\frac{\partial f}{\partial x}\right)^2}{1 + \left(\frac{\partial f}{\partial x}\right)^2 + f\frac{\partial^2 f}{\partial x^2}}. \tag{10}$$

Normal faulting in the hangingwall will preferentially take place at a point originally at a distance $x_{s,m}$ from the fault tip for which the stretch at the surface is maximum, that is where

$$\frac{\partial \Lambda_s}{\partial x_f} = 0. \tag{11}$$

Using equation (7) for $f(x)$ and after some tedious algebra, one may derive the following expression for $x_{s,m}$:

$$x_{s,m} = x_{f,m} + \frac{z_0^2}{\lambda}\left[1 - \exp\left(-\frac{x_{f,m}}{\lambda}\right)\right]\exp\left(-\frac{x_{f,m}}{\lambda}\right), \tag{12}$$

where

$$x_{f,m} = \lambda \ln\left[\frac{2\left[\left(\frac{z_0}{\lambda}\right)^2 + 1\right]}{-1 + \sqrt{1 + 4\left[\left(\frac{z_0}{\lambda}\right)^2 + 1\right]}}\right], \tag{13}$$

or, in terms of dimensionless variables $\bar{x}_{s,m} = (x_{s,m}/\lambda)$ and $\bar{z}_0 = (z_0/\lambda)$:

$$\begin{cases} \bar{x}_{s,m} = \bar{x}_{f,m} + \bar{z}_0^2 [1 - \exp(-\bar{x}_{f,m})] \exp(-\bar{x}_{f,m}) \\ \bar{x}_{f,m} = \ln\left[\dfrac{2(\bar{z}_0^2 + 1)}{-1 + \sqrt{1 + 4(\bar{z}_0^2 + 1)}}\right] \end{cases} \quad (14)$$

Note that $\bar{z}_0$ is equal to the tangent of the dip of the fault where it intersects the surface.

We can therefore predict the approximate normalized distance, $\bar{x}_{s,m}$, from the so-called crestal graben to the hangingwall tip, as a function of the tangent of the slope of the fault at the surface, $\bar{z}_0$. This relationship, shown in Fig. 8, indicates that $\bar{x}_{s,m}$ is inversely proportional to $\bar{z}_0$. The vertical bar in Fig. 8 is the limit beyond which the rule of the normal fails as some points within the hangingwall are intersected by normals from several parts of the detachment fault.

Dilatation

So far, the kinematic model has assumed that the distance from any point within the hangingwall to the fault is preserved during deformation so that the stretch, Λ_0, is restricted to a direction perpendicular to the fault normal. This implies unrealistic levels of dilatation in some circumstances. The kinematic model may be refined to include a condition of incompressibility such that the deformation of the hangingwall is non-dilatational. Since we are only working in two dimensions, incompressibility implies that there should be a component of stretch in the direction of the normal, Λ_n, such that:

$$\Lambda_n \Lambda_0 = 1. \quad (15)$$

The condition of incompressibility is added to the kinematic model by rectifying the computed final position of a particle, $x_1(X)$, along the normal to the fault surface. The total tangential stretch, Λ_0, is then given by:

$$\Lambda_0 = \frac{1 - \dfrac{r^*}{\Gamma_2}}{1 - \dfrac{r}{\Gamma_1}}, \quad (16)$$

where r^* is the 'rectified' distance from the fault after isochoric deformation. r^* may be computed by integrating the stretch Λ_n along the normal from the fault surface:

$$r^* = \int_0^r \Lambda_n \, dr' = \int_0^r \frac{dr'}{\Lambda_0} = \int_0^r \frac{1 - \dfrac{r'}{\Gamma_1}}{1 - \dfrac{r^*}{\Gamma_2}} dr'. \quad (17)$$

This integral equation in r^* may be transformed into the following differential equation with no loss of generality:

$$\frac{\partial r^*}{\partial r} = \frac{1 - \dfrac{r}{\Gamma_1}}{1 - \dfrac{r^*}{\Gamma_2}}. \quad (18)$$

The general solution of this is:

$$r^* = \Gamma_2 - \sqrt{\Gamma_2^2 - 2\Gamma_2 r + r^2 \frac{\Gamma_2}{\Gamma_1} + C}, \quad (19)$$

where C is an arbitrary constant. Because points that are originally located on the fault surface remain on the fault surface after deformation ($r = 0 \rightarrow r^* = 0$), $C = 0$. The 'rectified' tangential stretch, Λ_0, is therefore given by:

$$\Lambda_0 = \frac{\sqrt{1 - 2\dfrac{r}{\Gamma_2} + \dfrac{r^2}{\Gamma_1 \Gamma_2}}}{1 - \dfrac{r}{\Gamma_1}}. \quad (20)$$

This modification to the kinematic model is, in fact, the generalization of the area-corrected version of the slip-line model developed by Wheeler (1987).

The results shown in Fig. 7 have been re-computed incorporating the condition of incompressibility and are displayed in Fig. 9. The main difference is the subsidence of the surface in the region of maximum extension, that is the crestal graben. The predicted hangingwall geometry may be once again compared with the results of the two-dimensional experiments (Fig. 3) confirming that the condition of incompressibility has improved the predictions of the kinematic model: the surface of the hangingwall subsides in regions of finite extension.

That the amount of surface subsidence observed in the scaled experiment is smaller than the predictions of the dilatation-corrected kinematic model suggests that deformation of the sand pack was not purely isochoric.

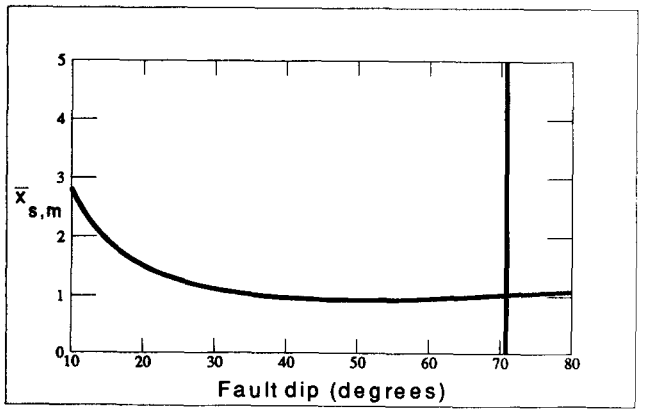

Fig. 8. Position of the crestal graben, $\bar{x}_{s,m}$ as a function of the fault dip at the surface measured from the hangingwall tip and normalized by the fault soling depth, z_0, as derived from the kinematic model; the region of the curve to the right of the vertical line corresponds to fault geometries where the rule of the normal cannot be applied.

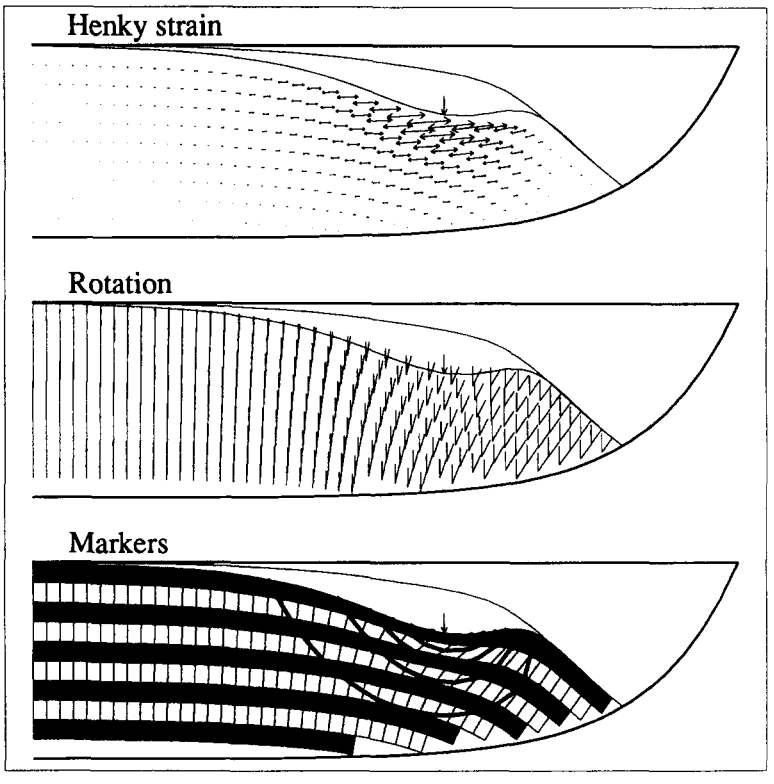

Fig. 9. Results of the kinematic model similar to those of Fig. 7 but including the condition of incompressibility.

GENERALIZATION OF THE RULE OF THE NORMAL TO THREE DIMENSIONS

The generalization of the rule of the normal to the three-dimensional case is straightforward. Difficulties only arise in regions of the hangingwall where more than one normal to the fault surface exist. For the fault geometry used in the analogue three-dimensional experiments (Fig. 2b), this situation arises in the vicinity of the plane of symmetry in the center of the model (region C of Fig. 4), where two (and only two) normals intersect, one from each segment of the fault surface. The ambiguity, similar to the one arising in two dimensions from steep fault situations, was removed in the following manner: two new particle locations, $x_{1,a}(X)$ and $x_{1,b}(X)$ are computed by applying the rule of the normal along both segments of the fault surface. The final particle location, $x_1(X)$, is set to be a weighted average of $x_{1,a}$ and $x_{1,b}$, where the weighting factors are chosen to avoid discontinuities in the kinematic model.

An analytical expression for the stretch and rotation tensors, Λ and Ω, cannot easily be derived in the three-dimensional case. We therefore computed numerically the deformation gradient, $F = (\partial X/\partial x)$. The deformation gradient was then split into its symmetrical part, the stretch tensor Λ, and its anti-symmetrical part, the rotation tensor Ω. This operation, called polar decomposition, is not straightforward in three dimensions, but can be performed at a minimal computational cost by making use of the Cayley–Hamilton theorem (Braun 1994).

The two principal components of the stretch tensor, Λ_1 and Λ_2, that lie in a plane perpendicular to the normal to the fault surface were computed in this way for a series of points originally at the surface of the hangingwall. The condition of incompressibility was then incorporated in the model using the following iterative method: (1) for every point, the final location was calculated without the constraint of incompressibility; (2) that position was rectified by adding a component to the stretch tensor in a direction normal to the fault surface, $\Lambda_n = (1/\Lambda_1\Lambda_2)$; (3) the deformation gradient was recomputed using the rectified position; and (4) if the new position differed from the previously calculated one, steps (2)–(4) were repeated.

The computed deformation of the surface of the hangingwall is shown in Figs. 10(a) & (b) and may be compared to the results of the three-dimensional analogue experiment (Fig. 4). The kinematic model again reproduces all the characteristics of the deformation field observed in the analogue experiment; in particular:

—symmetry about the centre line;

—a very flat surface over the proximal regions P1 and P2 of the hangingwall undergoing substantial solid-body rotation;

—extension normal to the fault trace in regions T1 and T2 of the hangingwall;

—almost pure horizontal translation without internal deformation in the distal regions D1 and D2;

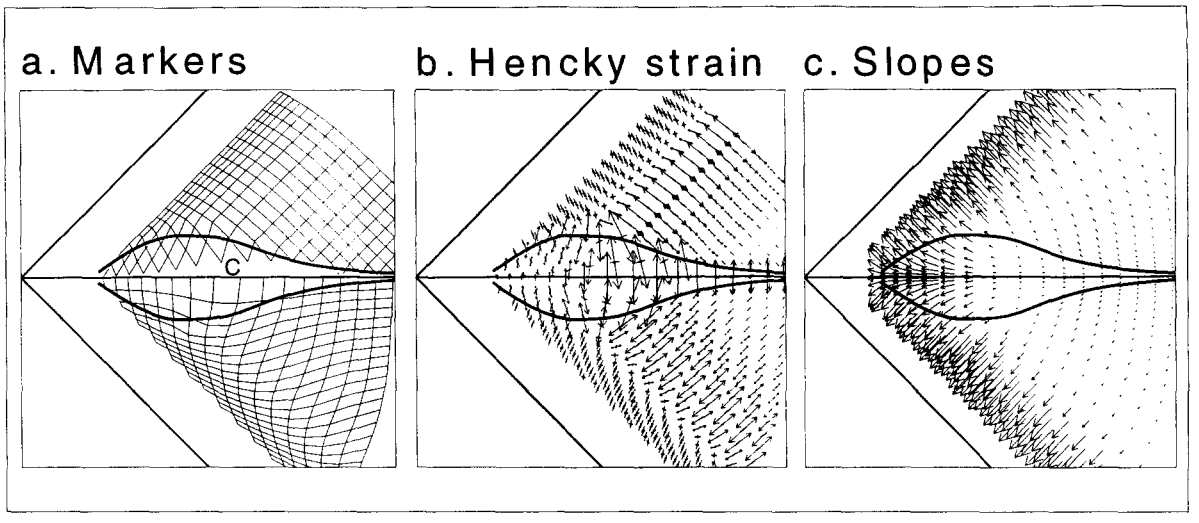

Fig. 10. Results of the three-dimensional kinematic model. (a) Geometry of an originally regular grid following deformation. As in the sand box experiment, the grid was parallel to the fault trace on the left-hand side region of the hangingwall and parallel to the edges of the box on the right-hand side. The region labelled C between the two thick black lines is the region of the sand pack where there exist two normals to the fault. (b) Distribution of deformation at the surface of the hangingwall. The arrows are aligned along the direction of the local maximum stretch components and their amplitude is given by the value of the Hencky strain in that direction. (c) Computed surface slopes; the direction of the arrows indicate the direction of the local maximum dip and their magnitudes indicate the relative dip.

—extension in a direction perpendicular to the direction of imposed displacement in the central region (C). Note that region C corresponds to the portion of the hangingwall where normals to both fault segments cross.

FRICTION ALONG THE FAULT SURFACE

The rule of the normal is based on the assumption that the deformation of the hangingwall is dominated by unfolding to conform with the shape of the detachment. This assumption is correct in situations where there is no drag along the fault. In the analogue experiments, the presence of the mylar sheet ensures that frictional tractions do not cause internal deformation of the sand pack. However, in nature drag is an intrinsic part of fault movement and in some, if not most, cases it cannot be neglected.

Our kinematic model cannot properly address the dynamic problem of fault friction; however it may be easily modified to include non-uniform displacement along the fault surface including that which would result from friction. This is done by introducing an extra parameter in the model: the displacement of the tip of the hangingwall, $u_t < u_0$, where u_0 is the displacement of the hangingwall far away from the fault tip. To avoid introducing an additional length scale in the model, we parameterize the displacement along the fault surface in the following manner:

$$u = u_t + (u_0 - u_t)\frac{z}{f(x=\infty)} = u_t + (u_0 - u_t)\frac{f(x)}{f(\infty)}. \quad (21)$$

This differential movement along the fault surface gives rise to an additional tangential stretch, Λ_f, expressed as:

$$\Lambda_f = 1 + \frac{\partial u}{\partial s}, \quad (22)$$

where s is the distance measured along the surface:

$$s = \int_0^x \sqrt{1 + \left(\frac{\partial f}{\partial x}\right)^2}\, dx. \quad (23)$$

Λ_f may also be expressed directly in terms of $\partial f/\partial x$ in the following manner:

$$\Lambda_f = 1 + \frac{(u_0 - u_t)}{f(\infty)} \frac{\frac{\partial f}{\partial x}}{\sqrt{1 + \left(\frac{\partial f}{\partial x}\right)^2}}. \quad (24)$$

In the two-dimensional case, the total tangential stretch resulting from the deformation is therefore:

$$\Lambda_0 = \Lambda_f \frac{1 - \frac{r^*}{\Gamma_2}}{1 - \frac{r}{\Gamma_1}}, \quad (25)$$

and, including the condition of incompressibility:

$$\Lambda_0 = \frac{\sqrt{\Lambda_f^2 - 2\frac{r\Lambda_f}{\Gamma_2} + \frac{r^2\Lambda_f}{\Gamma_1\Gamma_2}}}{1 - \frac{r}{\Gamma_1}}. \quad (26)$$

Figures 11(a)–(c) show the internal deformation field derived from the kinematic model where $u_t = u_0$, $u_t = (u_0/2)$ and $u_t = 0$, respectively. In cases where $u_t \neq u_0$ (Figs. 11b & c), the extension and the associated subsidence are distributed over a wider area than in the case where $u_t = u_0$ (Fig. 11a) but the position of the crestal graben is only slightly affected. The quantities u_t and u_0 may be determined independently by measuring fault

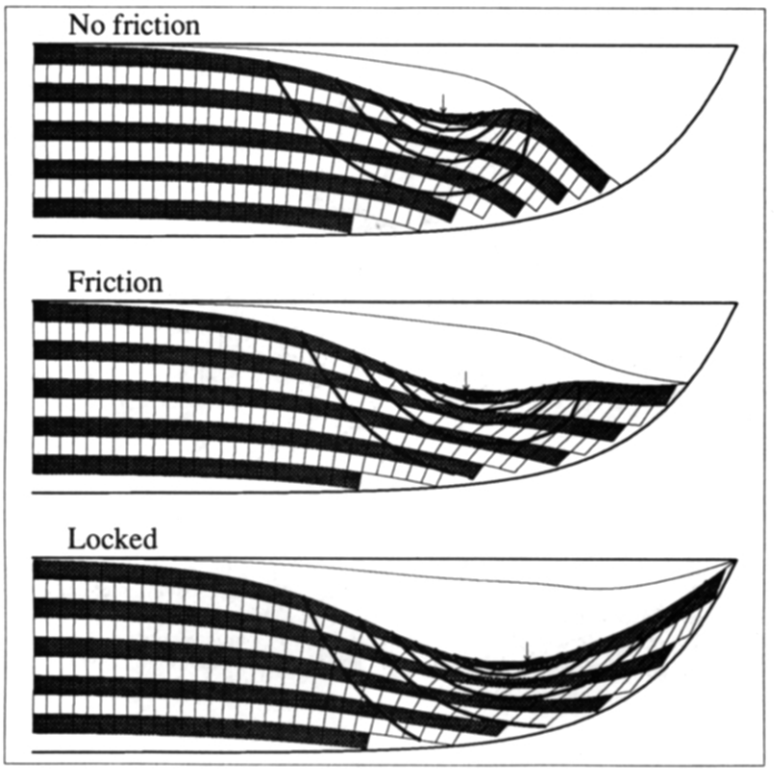

Fig. 11. Results of the kinematic model similar to Fig. 9(c) but including fault drag as an imposed difference between displacement along the fault at the tip of the hangingwall block, u_t, and along the flat region of the fault surface, u_0. (a) $u_t = u_0$. (b) $u_t = (u_0/2)$. (c) $u_t = 0$. The small vertical arrows indicate the location of the maximum surface extension as computed from the rule of the normal.

displacement at the tip of the fault and far away from the tip of the fault (preferably where the fault is flat) respectively, although, in practice, this might be difficult to achieve.

NON-SYMMETRICAL FAULT SURFACE AND DIP ANALYSIS

The use of dip analysis to infer kinematic histories in regions of crustal extension potentially provides a powerful alternative to the classical, but effectively two-dimensional and idealized, use of fault geometries predicted by orthogonal extension (Lister *et al.* 1986) and strike-slip motion (Aydin & Nur 1982, Mann *et al.* 1983, Sylvester 1988) models for basin formation. Essentially, dip analysis is based on the assumption that the dip direction of rotated blocks of acoustic basement in the hangingwall above the main detachment surface corresponds to the direction of extension or tectonic transport (Scott *et al.* 1994). Dip analysis is therefore independent of known or interpreted fault geometries and is suitable for non-ideal oblique-slip extensional terranes (Scott *et al.* 1992). Dip analysis relies, however, on the assumption that the dip direction of the surface of hangingwalls is consistent over an extensional domain and corresponds to the direction of extension or tectonic transport, regardless of the orientation or shape of the extension-accommodating fault surface.

To test this hypothesis, we use the result of the three-dimensional scaled laboratory experiments described

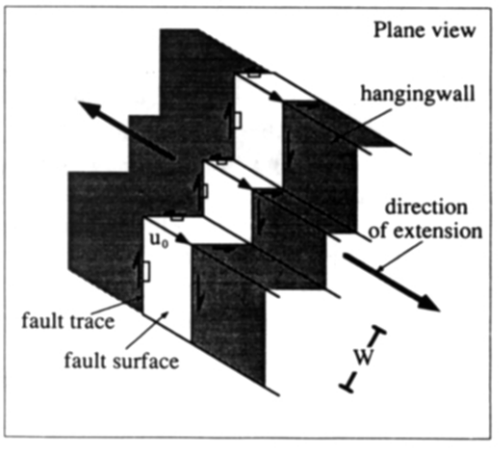

Fig. 12. Plan view of a conceptual oblique-slip extensional terrane. The direction of extension is not aligned perpendicular to the strike of pre-existing faults. Therefore, extension results in dip-slip and strike-slip movement on all fault segments. W is the average length of fault segments.

above. Indeed, the fault geometry used in the experiment represents the general situation shown in Fig. 12, where crustal extension is accommodated by oblique-slip along a series of randomly oriented fault segments. Such a 'general' extensional terrane may be characterized by: (1) a depth to detachment, z_0, assumed common to all fault segments; (2) a segmentation length scale, W, or average length of fault segments; and (3) a listricity scale, λ, or average inverse curvature of fault segments. The question we wish to answer is then: in which region of the (z_0, W, λ) space is dip analysis accurate in

providing an estimate of the direction of tectonic transport?

The results of the three-dimensional scaled experiments clearly showed that, in the case where the fault surface is symmetrical with respect to the direction of tectonic transport, the central region (C) of the hangingwall dips in a direction aligned with the direction of tectonic transport. This result is confirmed by the kinematic model as shown in Fig. 10(c). The dip vectors computed at the surface of the hangingwall by using the rule of the normal are practically aligned with the direction of extension within the central region (C) whereas they follow exactly the dip of each fault segment anywhere else. This result may be generalized to non-symmetrical fault geometries: the dip of region C is, regardless of the degree of symmetry of the fault surface, aligned with the direction of tectonic transport.

We can therefore conclude that the dip analysis method provides a reasonably accurate estimate of the direction of tectonic transport if the dip measurements are restricted to the central region C of the hangingwall surface. Dip measurements made outside of region C will yield apparent estimates of the direction of tectonic transport aligned with the direction of dip of each of the fault segments. The validity of dip analysis therefore depends on the proportion of the hangingwall surface that is comprised in region C. By assuming that region C is the surface expression of the region of the hangingwall where normals from each segment of the fault surface cross, we may compute its surface area, S^C, for a large range of parameter values. We derived the following relationship:

$$\frac{S^C}{z_0^2} \propto \tan \phi. \tag{27}$$

This relationship tells us that the surface area of region C mostly depends on z_0, the depth to detachment and ϕ, the dip of the 'master' fault. S^C does not depend on the angle that the master fault makes with the direction of tectonic displacement. Therefore, in an extensional terrane characterized by fault segmentation at a scale W, a depth to detachment z_0 and an average fault listricity λ, the use of the dip analysis method is justified if

$$z_0 > W \quad \text{and} \quad \lambda < W. \tag{28}$$

In other words, if extension-accommodating faults are steep and consist of short segments relative to the depth of detachment, dip analysis is justified as a means of constraining the tectonic transport direction. In the Tanganyika and Malawi rift zones of East Africa, normal to oblique slip border faults are steep (Rosendahl *et al.* 1988, Scholz *et al.* 1989) and apparently continue to deep levels (32 ± 5 km) as indicated by recent earthquake activity (Jackson & Blenkinsop in press). Segmentation of the main border faults is common as indicated by detailed mapping (Wheeler 1989), especially as they approach accommodation zones (Scott 1994). In this case, dip analysis provides a consistent kinematic picture (Scott *et al.* 1992).

DISCUSSION AND CONCLUSIONS

Summary of results

A series of two-dimensional scaled experiments have been conducted in an attempt to understand the internal deformation of a crustal block sliding along a listric normal fault. The results of the experiments closely resemble the deformation patterns observed by previous workers (e.g. Ellis & McClay 1988) in similarly scaled analogue experiments. As deformation proceeds, a large antiform topped by an extensional graben forms in the hangingwall at some distance from the fault tip whereas the hangingwall block head deforms by pure rigid-body rotation.

The experiments were then extended to the three-dimensional case using a fault surface made of two symmetrical listric segments. The results resemble those of the two-dimensional experiments in that the regions nearest to the fault tip deform by rigid-body rotation and two crestal-grabens develop to accommodate extension perpendicular to the fault segments. Along the axis of symmetry, however, extension in the hangingwall is perpendicular to the direction of imposed displacement.

We have developed a simple kinematic model based on the rule of the normal, a generalization of the slip-line construction of Williams & Vann (1987). The kinematic model reproduces in detail the deformation field observed in the two- and three-dimensional experiments, supporting the conclusion of Ellis & McClay (1988) that the deformation of the hangingwall is quasi-independent of its mechanical behaviour and is solely determined by the shape of the fault surface.

An additional parameter has been introduced in the kinematic model: the displacement of the hangingwall at its head, assumed to be different from the displacement of the block along the flat portion of the fault surface. This modification to the kinematic model adds some drag fold character near the head of the hangingwall, but the other characteristics of the extensional deformation are only slightly modified.

The results of the analogue experiments and the kinematic model support the use of dip analysis to estimate the direction of tectonic transport in oblique-slip extensional terranes as suggested by Scott *et al.* (1992). This is particularly true in cases where the depth to detachment is greater than the average fault segmentation length and where the average fault listricity is smaller than the segmentation length.

Ramp–flat–ramp fault geometry

The results of the analogue experiments and the kinematic model based on the rule of the normal demonstrate that, although the internal deformation of the hangingwall is solely controlled by the geometry of the fault surface, the geometry of the hangingwall surface is not a direct reflection of the geometry of the fault surface. In all the cases presented here, the fault geometry was parameterized as a smooth, monotonic expo-

nential curve; despite that, the surface of the hangingwall after deformation displayed complex topography. Even in this simple situation where there is no drag along the fault and dilatation in the hangingwall is permitted, the hangingwall surface topography predicted by the kinematic model is not monotonic. When the constraint of incompressibility is added to the kinematic model, the predicted surface topography is characterized by a well-defined trough overlying the region of maximum extension. Our results therefore suggest that care should be taken before interpreting extensional collapse in the hangingwall as the result of a ramp–flat–ramp geometry in the fault surface as suggested by Gibbs (1984).

Acknowledgements—The authors wish to thank K. Lambeck and R. Kerr for the useful suggestions they made during the construction and set up of the deformation apparatus, Dan Schultz-Ela and an anonymous reviewer for constructive comments they made on an earlier version of this manuscript. Part of this work was done while Geoff Batt was a Vacation Scholar at the Research School of Earth Sciences of the Australian National University.

REFERENCES

Aydin, A. & Nur, A. 1982. Evolution of pull-apart basins and their scale independence. *Tectonics* **1**, 91–105.

Braun, J. 1994. Three-dimensional numerical simulations of crustal-scale wrenching using a non-linear failure criterion. *J. Struct. Geol* **16**, 1173–1187.

Dula, W. F. 1991. Geometric models of listric normal faults and rollover folds. *Am. Ass. Petrol. Geol.* **75**, 1609–1625.

Ellis, P. G. & McClay, K. R. 1988. Listric extensional fault systems—results of analog model experiments. *J. Basin Res.* **1**, 55–70.

Fung, Y. C. 1965. *Foundations of Solid Mechanics*. Prentice-Hall, London.

Gibbs, A. D. 1984. Structural evolution of extensional basin margins. *J. geol. Soc. Lond.* **141**, 609–620.

Horsfield, W. T. 1977. An experimental approach to basement controlled faulting. *Geologie Mijnb.* **56**, 363–370.

Hubbert, M. K. 1937. Theory of scale models as applied to the study of geological structures. *Bull. geol. Soc. Am.* **48**, 1459–1520.

Jackson, J. & Blenkinsop, T. In press. The Malawi earthquake of March 10, 1989: deep faulting within the East African Rift System. *Tectonics* **12**.

Jaeger, J. C. & Cook, N. G. W. 1979. *Fundamental of Rock Mechanics* (3rd edn). Chapman and Hall, London.

Lister, G. S., Etheridge, M.A. & Symonds, P.A. 1986. Detachment faulting and the evolution of passive continental margins. *Geology* **14**, 245–250.

Mann, P., Hempton, M. R., Bradley, D. C. & Burke, K. 1983. Development of pull-apart basins. *J. Geol.* **91**, 529–554.

McClay, K. R. 1989. Physical models of structural styles during extension. In: *Extensional Tectonics and Stratigraphy of the North Atlantic Margins* (edited by Tankard, A. J. & Balkwill, H. R.). *Mem. Am. Ass. Petrol. Geol.* **46**, 95–110.

McClay, K. R. & Ellis, P. G. 1987a. Analogue models of extensional fault geometries. In: *Continental Extensional Tectonics* (edited by Coward, M. P., Dewey, J. F. & Hancock, P.L.). *Spec. Publs geol. Soc. Lond.* **28**, 109–125.

McClay, K. R. & Ellis, P. G. 1987b. Geometries of extensional fault systems developed in model experiments. *Geology* **15**, 341–344.

Rosendahl, B. R., Versfelt, J. W., Scholz, C. A., Buck, J. E. & Woods, L. D. 1988. Seismic atlas of Lake Tanganyika, East Africa. *Proj. PROBE Geophys. Atlas Ser.* **1**. Duke University, Durham, North Carolina.

Scholz, C. A., Rosendahl, B. R., Versfelt, J. W., Kaczmarick, K. J. & Woods, L. D. 1989. Seismic atlas of Lake Malawi (Nyasa), East Africa. *Proj. PROBE Geophys. Atlas Ser.* **2**. Duke University, Durham, North Carolina.

Scott, D. L. 1994. Oblique lithospheric extension: a comparative analysis of the East African rift system and some Australian passive margins. Unpublished Ph.D. thesis, Australian National University, Canberra, Australia.

Scott, D. L., Braun, J. & Etheridge, M. A. 1994. Dip analysis as a tool for estimating regional kinematics in extensional terranes. *J. Struct. Geol.* **16**, 393–401.

Scott, D. L., Etheridge, M. A. & Rosendahl, B. R. 1992. Oblique-slip deformation in extensional terrains: a case study from the lakes Tanganyika and Malawi rift zones, East Africa. *Tectonics* **11**, 998–1009.

Sylvester, A. G. 1988. Strike-slip faults. *Bull. geol. Soc. Am.* **100**, 1666–1703.

Verral, P. 1981. Structural interpretation with application to North Sea problems. *Joint Ass. Petrol. Expl. Courses (U.K.), Course Notes* **3**.

Wheeler, J. 1987. Variable-heave models of deformation above listric normal faults: the importance of area conservation. *J. Struct. Geol.* **9**, 1047–1049.

Wheeler, W. H. 1989. The Livingstone Mountains border fault system, Lake Nyasa (Maqlawi), East Africa: a case study of an oblique-slip rift basin border fault from onshore and sub-surface perspectives. Unpublished M.Sc. thesis, Duke University, Durham, North Carolina.

White, N.J., Jackson, J. A. & McKenzie, D.P. 1986. The relationship between the geometry of normal faults and that of the sedimentary layers in their hanging walls. *J. Struct. Geol.* **8**, 897–909.

Williams, G. & Vann, I. 1987. The geometry of listric normal faults and deformation in their hanging-walls. *J. Struct. Geol.* **9**, 789–795.